

# Force approach for the pseudopotential lattice Boltzmann method

L. E. Czelusniak<sup>1,\*</sup>, V. P. Mapelli<sup>1</sup>, M. S. Guzella<sup>2</sup>, L. Cabezas-Gómez<sup>1</sup>, and Alexander J. Wagner<sup>3</sup>

<sup>1</sup>*Heat Transfer Research Group, Department of Mechanical Engineering,*

*São Carlos School of Engineering, University of São Paulo, São Carlos, SP, Brazil*

<sup>2</sup>*Institute of Science and Technology, Federal University of*

*Jequitinhonha and Mucuri Valleys, UFVJM, Diamantina, MG, Brazil*

<sup>3</sup>*Department of Physics, North Dakota State University, Fargo, North Dakota 58108, USA*

(Dated: March 19, 2020)

The pseudopotential method is one of the most popular extensions of the lattice Boltzmann method (LBM) for phase change and multiphase flow simulation. One attractive feature of the original proposed method consists on its simplicity of adding a force dependent on a nearest-neighbor potential function, which became known as the Shan-Chen interaction force. Some of the well known drawbacks implied by this method involves lack of thermodynamic consistency and impossibility to control the surface tension independently. In order to correct these deficiencies, different approaches were developed in the literature, such as multirange interactions potential, which involves larger stencils than nearest-neighbor approach, and modified forcing schemes. In this work, a strategy is developed to control the liquid-gas density ratio and the surface tension by means of an appropriate interaction force field using only nearest-neighbor interactions. The proposed procedure is devised starting from the desired pressure tensor, which allow for the control of the equilibrium multiphase properties such as liquid-gas coexistence curve and surface tension. Then, it is shown how to derive an external force field able to replicate the effects of this pressure tensor in the macroscopic conservation equations. The final step of our procedure is implementing this external force in the LBE by using the classical Guo forcing scheme. Numerical tests regarding static and dynamic flow conditions were performed. Results obtained from simulations showed good agreement with expected analytical values. Most divergent solution observed was the droplet oscillation period under certain flow conditions, which deviated 9% from expected analytical result. The observed results corroborate that the proposed method is able to replicate the desired macroscopic multiphase behaviour.

## I. INTRODUCTION

The lattice Boltzmann method (LBM) [1] has grown as an alternative tool for fluid flow simulation. Differently from other numerical methods based on a direct discretization of the conservation equations, the LBM is based on a discretized form of the Boltzmann transport equation known as the lattice Boltzmann equation (LBE) [2]. In particular, for phase change phenomena and multiphase flow simulation, several models were developed within the LBM framework [3–6]. One of the most popular is the pseudopotential method [5, 7]. It consists in the definition of an artificial interaction potential which is capable of inducing phase separation. In this way, it is not necessary to track the interface between multiple phases as they are maintained by the short-range attraction force imposed to the fluid. This type of procedure is called diffuse interface modeling [8], since the density field varies continuously between the different phases due to the action of the force field, instead of having an exact interface location.

The original pseudopotential method was developed by Shan and Chen [5]. The authors proposed an interaction force that could maintain different phases in equilibrium. The drawbacks of this procedure involves lack of thermodynamic consistency and non-adjustable surface

tension. In a subsequent work, Shan and Chen [7] focused on the macroscopic behavior of their method. The authors addressed the effects of the proposed interaction force into the pressure tensor. With this approach, the authors were able to study the equilibrium properties of a fluid governed by this resulting pressure tensor. It is known that in diffuse interface models, the pressure tensor plays a key role in the phase-change process, controlling liquid-gas density ratio and surface tension [9]. A different interaction force was proposed by Zhang and Chen [10], but this model suffers from the same issues of the Shan and Chen approach. The first improvement was done by Kupershtokh *et al.* [11], who were able to adjust the liquid-gas coexistence curve by combining the previous interaction forces. However, this technique was still not able to allow controlling surface tension without affecting the liquid-gas densities. A similar procedure was also proposed later [12]. This technique allowed successful applications of LBM to multiphase simulations, such as simulations of pool boiling [13, 14].

The procedures aforementioned are classified as nearest neighbor interaction forces, since their implementation requires only information from the fluid properties at the nodes adjacent to the node of interest. One of the further attempts to enhance multiphase behavior consists in the multirange interaction forces [15], which use larger numerical stencils involving nodes at greater distances. Sbragaglia *et al.* [16] proposed a multirange model capable of adjusting the liquid-gas density curve and the surface tension. However, Li and Luo [17] noticed that

---

\* luiz.czelusniak@usp.br

this model had some issues, since the density ratio of the system varied considerably with the change in surface tension. Recently, Kharmiani *et al.* [18] proposed a consistent interaction potential that permits to control independently the liquid-gas density ratio and surface tension. But one of the terms that constitutes the proposed force is calculated in two steps and it can be argued that this procedure is equivalent to a multirange approach, since it requires information from distances greater than the adjacent nodes. The disadvantages of the multirange model involve being computationally more expensive and the boundary conditions need to be modified [19]. Besides that, considering a first principles approach mapping a Molecular Dynamics simulation onto the lattice Boltzmann framework [20] we will argue below, that interactions should only involve adjacent nodes in the vast majority of practical simulations.

In order to incorporate the effects of an external force field into the LBE, no matter if it is a nearest-neighbour or multirange approach, one may use numerical procedures known as forcing schemes. Very common examples from literature are the forcing schemes developed by Guo *et al.* [21], Shan and Chen [5], Kupershtokh [22] and Wagner [23]. The use of a suitable forcing scheme in a numerical solution has been shown to have great importance, since some authors have observed distinguished behaviors for different schemes, even when the same external force field was applied [24, 25]. Li *et al.* [24] identified that such distinct behaviors were caused by distinguished terms introduced into the pressure tensor by the forcing schemes, and that affected the multiphase properties of the method. Based on this finding, the authors proposed a source term for the LBE in order to change the pressure tensor and to control the liquid-gas coexistence curve of the pseudopotential method. Later, the procedure was extended to allow the surface tension control without affecting the liquid and vapor densities [17]. This procedure is very attractive because the numerical scheme involves only properties at the adjacent nodes, resulting in a computationally efficient method. Most subsequent approaches in the literature followed this reasoning [26–28]. Also, it was discovered that higher order discretization errors caused by the forcing schemes play a big role in multiphase flows [23, 26] and these errors must be taken into account for proper determination of the pressure tensor. These procedures based on the work of Li *et al.* [24] allowed many applications of the pseudopotential method [29–31].

Even though many theoretical developments in forcing schemes were achieved concerning the design of pressure tensors that allow the control of the desired equilibrium multiphase properties, this knowledge was still not properly employed to devise interaction forces to overcome the limitation of previous models [5, 10, 11]. Some attempts were done but they involve the use of multirange interactions which reduce the method computational efficiency. Based on the current developments in the pseudopotential literature, in this work, we developed a strategy to

control the liquid-gas density ratio and the surface tension by means of an appropriate interaction force field using only nearest-neighbor interactions, without resorting to a change in the forcing scheme. The procedure starts by considering the desired pressure tensor, which allows for the control of the equilibrium properties of the pseudopotential method. We then derive an external force field which replicates the effects of this pressure tensor in the momentum conservation equation. The final step of our procedure is implementing this external force in the LB method by using the classical forcing scheme developed by Guo *et al.* [21].

The present paper is organized as follows. In Sec. II, the theoretical background related to LBM and pseudopotential method will be briefly discussed, with particular focus on the pressure tensor role. In Sec. III A, a fundamental approach to analyze the form of the interaction force will be discussed. This analysis is used as a foundation for the argument that using adjacent nodes in the pseudopotential method suffices to practical simulations. Then, in Sec. III B, it will be shown how to discretize the terms of the desired pressure tensor using finite differences. Later, an interaction force will be devised to replicate the effect of the desired pressure tensor in the conservation equations as shown in Sec. III C. Numerical simulations will be presented in Sec. IV to validate the proposed interaction force. Finally, a brief conclusion drawn from theoretical and numerical studies will be made in Sec. V.

## II. THEORETICAL BACKGROUND

### A. The Lattice Boltzmann Equation

The LBE can be written as:

$$f_i(t+1, \mathbf{x} + \mathbf{c}_i) - f_i(t, \mathbf{x}) = \Omega_i(\mathbf{f}, \mathbf{f}^{eq}) + S_i, \quad (1)$$

where  $f_i$  are the particle distribution functions related with the velocity  $\mathbf{c}_i$  and  $\mathbf{f}$  is a vector with components  $[\mathbf{f}]_i = f_i$ . Also,  $t$  and  $\mathbf{x}$  are the time and space coordinates, respectively. The term  $\Omega_i(\mathbf{f}, \mathbf{f}^{eq})$  is the collision operator and it is, in general, dependent on  $\mathbf{f}$  and the equilibrium distribution function,  $\mathbf{f}^{eq}$ . For the two-dimensional nine velocities set (D2Q9), the velocities  $\mathbf{c}_i$  are given by:

$$\mathbf{c}_i = \begin{cases} (0, 0), & i = 0, \\ (1, 0), (0, 1), (-1, 0), (0, -1), & i = 1, \dots, 4, \\ (1, 1), (-1, 1), (-1, -1), (1, -1), & i = 5, \dots, 8. \end{cases} \quad (2)$$

The simplest form of  $\Omega_i(\mathbf{f}, \mathbf{f}^{eq})$  is the single-relaxation time, also known as BGK collision operator [32], described in Eq. (3a). One can improve stability and to some extent accuracy by allowing different relaxation times for different modes. This is known as the

multi-relaxation time (MRT) collision operator, shown in Eq. (3b).

$$\Omega_i(\mathbf{f}, \mathbf{f}^{eq}) = -\frac{1}{\tau}(f_i - f_i^{eq}), \quad (3a)$$

$$\Omega_i(\mathbf{f}, \mathbf{f}^{eq}) = -[\mathbf{M}^{-1}\mathbf{\Lambda}\mathbf{M}]_{ij}(f_j - f_j^{eq}), \quad (3b)$$

where the parameter  $\tau$ , in Eq. (3a), is the relaxation time. In Eq. (3b),  $\mathbf{\Lambda}$  is the relaxation matrix and  $\mathbf{M}$  is the matrix that converts  $(\mathbf{f} - \mathbf{f}^{eq})$  into a set of moments. The particular form of these matrices can vary, as discussed by Kaehler and Wagner [33], but the hydrodynamic modes of mass, momentum, and stress tensor have to be eigenvectors of the collision matrix. The eigenvalues of this matrix then represent now a set of relaxation times that can be different for the different eigenvectors. The MRT collision operator has been widely used in multi-phase simulations [29, 34, 35]. Note that the MRT equation recovers the BGK collision operator if all relaxation times of the MRT collision operator are equal. The form of the matrices  $\mathbf{M}$  and  $\mathbf{\Lambda}$  are presented in Appendix A.

A popular form of the equilibrium distribution function is:

$$f_i^{eq} = w_i \left( \rho + \frac{c_{i\alpha}}{c_s^2} \rho u_\alpha + \frac{(c_{i\alpha}c_{i\beta} - c_s^2\delta_{\alpha\beta})}{2c_s^4} \rho u_\alpha u_\beta \right), \quad (4)$$

where the terms  $w_i$  are the weights related with each velocity  $\mathbf{c}_i$ , and  $c_s$  is the lattice sound speed. For D2Q9 set, the weights  $w_i$  are given by  $w_0 = 4/9$ ,  $w_{1,2,3,4} = 1/9$  and  $w_{5,6,7,8} = 1/36$ , and  $c_s$  is equal  $1/\sqrt{3}$ . Also,  $\rho$  and  $\mathbf{u}$  are the fluid density and velocity, respectively given by (7a) and (7b).

The last term in the right-hand side of Eq. (1),  $S_i$ , is what defines the forcing scheme, i.e. this term is responsible for adding the effects of an external force field,  $F_\alpha$ , in the recovered macroscopic conservation equations. One of the most widely used forcing scheme in literature was developed by Guo *et al.* [21], and it can be described as follows:

$$S_i = C_{ij}w_j \left( \frac{c_{j\alpha}}{c_s^2} F_\alpha + \frac{(c_{j\alpha}c_{j\beta} - c_s^2\delta_{\alpha\beta})}{c_s^4} F_\alpha u_\beta \right), \quad (5)$$

where the term  $C_{ij}$  depends on whether the BGK, Eq. (6a), or the MRT, Eq. (6b), collision operator is being used. Both definitions can, respectively, be given by:

$$C_{ij} = \left( 1 - \frac{1}{2\tau} \right) \delta_{ij}, \quad (6a)$$

$$C_{ij} = \left[ \mathbf{M}^{-1} \left( \mathbf{I} - \frac{\mathbf{\Lambda}}{2} \right) \mathbf{M} \right]_{ij}, \quad (6b)$$

where  $\mathbf{I}$  is the identity matrix. The relation between particle distribution functions  $f_i$  and the actual fluid velocity  $\mathbf{u}$  depends on the forcing scheme. For the Guo *et al.*

forcing scheme, density and velocity fields are given by:

$$\rho = \sum_i f_i, \quad (7a)$$

$$\rho \mathbf{u} = \sum_i f_i \mathbf{c}_i + \frac{\mathbf{F}}{2}. \quad (7b)$$

The momentum density shown in Eq. (7b) needs to take into account the force field term,  $\mathbf{F}/2$ , in order for the numerical scheme to recover second-order accurate conservation equations under the influence of an external force field.

The LBE describes the evolution of particle distribution functions, however, the variables of interest are the macroscopic flow fields. The correspondence between the LBE and the macroscopic behavior that it simulates can be shown through different approaches. The standard procedure is the Chapman-Enskog analysis, and one alternative is the recursive substitution developed by Wagner [36] and further developed by Holdych *et al.* [37] and Kaehler and Wagner [33]. Up to second order terms, both procedures result in the same behavior, and it is not known if differences at higher orders will occur. Either approach recovers the mass and momentum conservation equations to second order:

$$\partial_t \rho + \partial_\alpha (\rho u_\alpha) = 0, \quad (8a)$$

$$\partial_t (\rho u_\alpha) + \partial_\beta (\rho u_\alpha u_\beta) = -\partial_\beta p_{\alpha\beta} + \partial_\beta \tau_{\alpha\beta} + F_\alpha, \quad (8b)$$

where the stress tensor,  $\tau_{\alpha\beta}$ , is given by  $\tau_{\alpha\beta} = \rho c_s^2 (\tau - 0.5)(\partial_\beta u_\alpha + \partial_\alpha u_\beta)$  for the BGK collision operator, Eq. (3a). The pressure tensor is given by  $p_{\alpha\beta} = \rho c_s^2 \delta_{\alpha\beta}$ . When MRT collision operator is applied, it is possible to adjust the bulk and shear viscosity independently in the stress tensor, since a greater number of relaxation times are used. A more thorough analysis applying the MRT collision operator can be seen in the work of Kaehler and Wagner [33].

Even though the LBE recovers the correct form of the Navier-Stokes up to second order terms, several studies have shown that the third order spatial discretization errors due to the forcing scheme play an important role in pseudopotential methods. These errors must be taken in account for the correct multiphase behavior prediction of the method. Third order analysis of the LBE considering different forcing schemes have been carried out in the LB literature. Zhai *et al.* [28], through Chapman-Enskog analysis, evaluated the recovered macroscopic equations up to the third order, considering the Guo *et al.* forcing scheme. Lycett-Brown and Luo [26] also investigated third order terms of a generic forcing scheme, using the technique developed by Holdych *et al.* From the results of these studies, one can show that third order discretization error produced by the Guo *et al.* forcing scheme is given by:

$$E_\alpha^{3rd} = \frac{c_s^2}{12} \partial_\beta \left[ (\partial_\gamma F_\gamma) \delta_{\alpha\beta} + \partial_\alpha F_\beta + \partial_\beta F_\alpha \right], \quad (9)$$

this term should be added in the right-hand side of Eq. (8b) in order to take into account the influence of higher order error in pseudopotential methods.

## B. Pressure Tensor and Phase Change

A common approach to address to multiphase lattice Boltzmann simulations is to define the force field to be implemented in LBE, and then to analyze the resulting pressure tensor, from which it is possible to draw conclusions of key multiphase features, such as equation of state, liquid-gas coexistence curve and surface tension.

In this work, we use a general pressure tensor as starting point, and show how it is related to multiphase flow properties. Afterwards, in next sessions, it is shown how it can be implemented through a discrete force in LBE, and how it is possible to devise a better method when compared to original Shan-Chen formulation.

A general pressure tensor from a single-phase pseudopotential method can be written as:

$$p_{\alpha\beta} = (c_s^2\rho + G\psi^2 + C_1G(\partial_\gamma\psi)(\partial_\gamma\psi) + C_2G\psi\partial_\gamma\partial_\gamma\psi) \delta_{\alpha\beta} + C_3G(\partial_\alpha\psi)(\partial_\beta\psi) + C_4G\psi\partial_\alpha\partial_\beta\psi, \quad (10)$$

where  $C_{1,2,3,4}$  are arbitrary coefficients,  $\psi$  is a density-dependent interaction potential,  $\psi = \psi(\rho)$ , and  $G$  is a parameter that controls the strength of interaction. One should notice that for a uniform state, the pressure tensor is simplified to  $p_{\alpha\beta} = (c_s^2\rho + G\psi^2) \delta_{\alpha\beta}$ . This term plays the role of the equation of state, and upon this fact, Yuan and Schaefer [38] proposed the following definition:

$$\psi = \sqrt{\frac{P_{EOS} - c_s^2\rho}{G}}, \quad (11)$$

where the term  $P_{EOS}$  represents any desired equation of state to be introduced into the method. When this technique is used, parameter  $G$  no longer controls the interaction strength, and it can be seen as an auxiliary parameter to keep the term inside the square root positive.

Observing the recovered momentum conservation equation in Eq. (8b), one may notice that what affects momentum balance is the divergence of the pressure tensor,  $-\partial_\beta p_{\alpha\beta}$ , and not the pressure tensor itself. Therefore, as pointed out by Sbragaglia *et al.* [16], different pressure tensors can reproduce identical hydrodynamic behaviors, as long as their divergences are equal to each other.

By applying the following tensor identity (for more details refer to Appendix B):

$$\partial_\beta [\psi\partial_\alpha\partial_\beta\psi - (\psi\partial_\gamma\partial_\gamma\psi)\delta_{\alpha\beta}] = \partial_\beta [(\partial_\gamma\psi)(\partial_\gamma\psi)\delta_{\alpha\beta} - (\partial_\alpha\psi)(\partial_\beta\psi)], \quad (12)$$

it is possible to show that the divergence of the tensor given by Eq. (10) is equivalent to the divergence of the

following pressure tensor:

$$p_{\alpha\beta} = (c_s^2\rho + G\psi^2 + A_1G(\partial_\gamma\psi)(\partial_\gamma\psi) + A_2G\psi\partial_\gamma\partial_\gamma\psi) \delta_{\alpha\beta} + A_3G\psi\partial_\alpha\partial_\beta\psi, \quad (13)$$

where  $A_{1,2,3}$  are arbitrary coefficients that obey the following relations:  $A_1 = C_1 + C_3$ ,  $A_2 = C_2 + C_3$  and  $A_3 = C_4 - C_3$ . The reduced form of pressure tensor, Eq. (13), is going to be used throughout the text.

A suitable problem to check liquid-gas coexistence curve and thermodynamic consistency obtained from the pressure tensor presented before is the planar interface between two phases in mechanical equilibrium [39]. Assuming  $x$  and  $y$  as the coordinates in, respectively, the normal and tangential direction to the interface, one may simplify the pressure tensor, once there is no gradients in  $y$ -direction, to:

$$p_{xx} = c_s^2\rho + G\psi^2 + G \left[ A_1 \left( \frac{d\psi}{dx} \right)^2 + (A_2 + A_3) \psi \frac{d^2\psi}{dx^2} \right], \quad (14a)$$

$$p_{yy} = c_s^2\rho + G\psi^2 + G \left[ A_1 \left( \frac{d\psi}{dx} \right)^2 + A_2 \psi \frac{d^2\psi}{dx^2} \right], \quad (14b)$$

$$p_{xy} = p_{yx} = 0. \quad (14c)$$

The mechanical equilibrium condition implies that the pressure tensor component  $p_{xx}$  must be constant and equal to the bulk pressure  $p_0$  along the  $x$  axis. By imposing this condition, Shan [39] deduced that the gas and liquid densities obtained by the pseudopotential method must satisfy the following relation:

$$\int_{\rho_g}^{\rho_l} (p_0 - c_s^2\rho - G\psi^2) \frac{\dot{\psi}}{\psi^{1+\epsilon}} d\rho = 0, \quad (15)$$

where  $\epsilon = -2A_1/(A_2 + A_3)$  and  $\rho_l, \rho_g$  are the densities of the liquid and vapor phases, respectively. The dot, as in  $\dot{\psi}$ , denotes the derivative with respect to density  $\rho$ . Another consequence of the equilibrium condition is that the bulk pressure of liquid and vapor regions far away from the interface must also be equal to  $p_0$ :

$$p_0 = c_s^2\rho_l + G[\psi(\rho_l)]^2, \quad (16a)$$

$$p_0 = c_s^2\rho_g + G[\psi(\rho_g)]^2. \quad (16b)$$

Together, Eqs. (15), (16a) and (16b) compose a well-posed problem that can be solved for  $p_0, \rho_l$  and  $\rho_g$ . In fact, this problem resembles the Maxwell equal-area rule, which states that for a given temperature, a thermodynamic consistent phase-change obeys the following gas-liquid density relation:

$$\int_{\rho_g}^{\rho_l} (p_0 - P_{EOS}) \frac{d\rho}{\rho^2} = 0. \quad (17)$$

By comparing Eqs. (17) and (15), [Lycett-Brown and Luo](#) were able to conclude that correct thermodynamic consistency will be achieved when:

$$\frac{\dot{\psi}}{\psi^{1+\epsilon}} d\rho \propto \frac{d\rho}{\rho^2}. \quad (18)$$

From Eq. (18) it is clear that the thermodynamic consistency of the pseudopotential method depends on the equation of state used to define the interaction potential and on parameter  $\epsilon$ , which in turn, are related to coefficients of pressure tensor.

Another important aspect of multiphase simulation is to properly control the surface tension. According to [Rowlinson and Widom \[40\]](#), the surface tension in diffuse interface models can be defined as:

$$\gamma = \int_{-\infty}^{\infty} (p_{xx} - p_{yy}) dx, \quad (19)$$

where, again,  $x$  and  $y$  are the interface normal and tangential directions, respectively. Equation (19) implies that the surface tension depends only on the anisotropic part of the pressure tensor. And, by consequence, it can be adjusted by the parameter  $A_3$ . For a planar interface, Eqs. (14a) and (14b) must be inserted into Eq. (19), resulting in the following relation:

$$\gamma_{pi} = \int_{-\infty}^{\infty} A_3 \psi \frac{d^2 \psi}{dx^2} dx, \quad (20)$$

In order to compute the surface tension of the planar interface case  $\gamma_{pi}$ , one can obtain the density profile that solve Eq. (14a) (for specific values of the parameters  $A_1$ ,  $A_2$  and  $A_3$ ) using a numerical method. This differential equation can be solved replacing the derivatives by finite difference approximations, as for example, second order central differences. The resultant nonlinear set of equations can be solved using Newton-Raphson method with the phase densities (obtained by solving Eq. (15)) at the borders as boundary conditions. With the knowledge of the density profile  $\rho(x)$ , the interaction potential profile is determined  $\psi(x) = \psi(\rho(x))$ . After that the surface tension can be computed using a numerical integration procedure to integrate Eq. (20).

### C. Shan-Chen method

The pseudopotential method originated when [Shan and Chen \[5\]](#) proposed a interaction force similar to:

$$F_{\alpha}^{SC} = -\psi(\mathbf{x}) \frac{2G}{c_s^2} \sum w_i \psi(\mathbf{x} + \mathbf{c}_i) c_{i\alpha}. \quad (21)$$

Using Taylor series expansion, a continuum form of the [Shan and Chen](#) force is obtained:

$$F_{\alpha}^{SC} = -G \left( \partial_{\alpha} \psi^2 + c_s^2 \psi \partial_{\alpha} \Delta \psi + \dots \right). \quad (22)$$

The momentum conservation equation, Eq. (8b), shows that the natural pressure tensor of the LBM is  $p_{\alpha\beta} = c_s^2 \rho \delta_{\alpha\beta}$ . Neglecting the higher order terms in Eq. (22), it is possible to introduce this force into the pressure tensor using the relation  $-\partial_{\beta} p_{\alpha\beta}^{SC} = -\partial_{\alpha} (\rho c_s^2 \delta_{\alpha\beta}) + F_{\alpha}^{SC}$ . The following relation is obtained:

$$p_{\alpha\beta}^{SC} = \left( c_s^2 \rho + G \psi^2 - \frac{c_s^2 G}{2} (\partial_{\gamma} \psi) (\partial_{\gamma} \psi) \right) \delta_{\alpha\beta} + c_s^2 G \psi \partial_{\alpha} \partial_{\beta} \psi. \quad (23)$$

This pressure tensor does not give the correct results for the coexistence curve. It is necessary to take into account the effect of the third order spatial discretization errors of the forcing scheme. For the [Guo \*et al.\*](#) forcing scheme, this error is given by Eq. (9).

It is possible to evaluate the new pressure tensor, by substituting Eq. (22) into Eq. (9). For simplification, here will be considered  $F_{\alpha}^{SC} \approx -G \partial_{\alpha} \psi^2$ . In this way, using Eq. (12), the discretization errors assume the form:

$$E_{\alpha}^{3rd} = -\partial_{\beta} \left( \frac{c_s^2 G}{2} (\partial_{\gamma} \psi) (\partial_{\gamma} \psi) + \frac{c_s^2 G}{2} \psi \partial_{\gamma} \partial_{\gamma} \psi \right) \delta_{\alpha\beta} = -\partial_{\beta} p_{\alpha\beta}^{3rd}, \quad (24)$$

where  $p_{\alpha\beta}^{3rd}$  is the effect caused by the third order discretization errors in the pressure tensor. Adding  $p_{\alpha\beta}^{3rd}$  to Eq. (23), the correct form of the pressure tensor for the pseudopotential method using the [Shan and Chen](#) force and the [Guo \*et al.\*](#) forcing scheme is obtained:

$$p_{\alpha\beta}^{SC} = \left( c_s^2 \rho + G \psi^2 + \frac{c_s^2 G}{2} \psi \partial_{\gamma} \partial_{\gamma} \psi \right) \delta_{\alpha\beta} + c_s^2 G \psi \partial_{\alpha} \partial_{\beta} \psi. \quad (25)$$

This highlights a key limitation of the Shan-Chen method: it is not possible to adjust the coexistence density curve, dependent on the pressure tensor, and the surface tension independently since they are both derived from the interaction potential  $\psi$ .

## III. INCORPORATING THE PRESSURE TENSOR INTO THE LBM

We propose a top-down approach to overcome the limitations inherent in the Shan-Chen method. The starting point is the complete pressure tensor, Eq. (13). Suitable force fields are devised to add the effect of the desired terms of this tensor into the recovered macroscopic conservation equations. Then, this interaction forces are directly discretized and later they are incorporated in the LBE.

In Sec. III A, we present a general inter-particle force for the pseudopotential model. After that, in Sec. III B, we discuss how to obtain numerical approximations to discretize the force terms. In Sec. III C we discuss the

method used to incorporate the effect of the desired pressure tensor in the recovered macroscopic conservation equation.

### A. Fundamental inter-particle force calculation

Originally the Shan-Chen method was developed with a microscopic interaction picture in mind. We review here an approach to make this relation more direct. A fundamental approach to analyze a lattice Boltzmann method is given by the Molecular Dynamics Lattice Boltzmann (MDLG) approach developed by Parsa *et al.* in [20]. The key idea here is to map a Molecular Dynamics (MD) simulation onto a lattice gas. The Boltzmann average of this lattice gas is then, in some sense, the most fundamental definition of a lattice Boltzmann method. This approach has proven useful in analyzing the fluctuations in non-ideal systems [41]. Here we use a theoretical approach to write down a fundamental representation of the lattice Boltzmann forcing term.

In a MD simulation, the conservative force  $\mathbf{F}$  on one particle is computed considering the potential energy  $V_{jk}$  between particles  $j$  and  $k$  by:

$$\mathbf{F}_j = - \sum_k \partial_{\mathbf{x}_k} V_{jk}(|\mathbf{x}_j - \mathbf{x}_k|). \quad (26)$$

Formally, we can write this as a continuous force field obtained from an integral over densities:

$$\mathbf{F}(\mathbf{x}, t) = \rho(\mathbf{x}, t) \int d\mathbf{x}' \rho(\mathbf{x}', t) \partial_{\mathbf{x}'} V(|\mathbf{x} - \mathbf{x}'|), \quad (27)$$

where we define the density as  $\rho(\mathbf{x}, t) = \sum_j \delta(\mathbf{x} - \mathbf{x}_j(t))$ . The key here is that in LB we have lattice cells that receive momentum from their neighboring cells. This is why we now coarse-grain the MD simulation onto a lattice. We define a discrete covering of lattice cells, and a function  $\Delta_\zeta(\mathbf{x})$  which indicates whether the position  $\mathbf{x}$  is contained in the lattice cell  $\zeta$ . We then integrate the force field over a lattice site to give:

$$\begin{aligned} \tilde{\mathbf{F}}(\zeta, t) &= \int d\mathbf{x} \mathbf{F}(\mathbf{x}, t) \Delta_\zeta(\mathbf{x}) \\ &= \int d\mathbf{x} \rho(\mathbf{x}, t) \Delta_\zeta(\mathbf{x}) \int d\mathbf{x}' \rho(\mathbf{x}', t) \partial_{\mathbf{x}'} V(|\mathbf{x} - \mathbf{x}'|), \end{aligned} \quad (28)$$

where the lattice space is represented by:

$$\Delta_\zeta(\mathbf{x}) = \begin{cases} 1, & \text{if } \mathbf{x} \text{ is in } \zeta \\ 0, & \text{else} \end{cases}.$$

Now in order to consider the interaction between particles from different lattice sites the last integral is translated into the next sum, which means that the space is now fully decomposed into lattice sites:

$$\begin{aligned} & \int d\mathbf{x}' \rho(\mathbf{x}', t) \partial_{\mathbf{x}'} V(|\mathbf{x} - \mathbf{x}'|) \\ &= \sum_\eta \int d\mathbf{x}' \rho(\mathbf{x}', t) \Delta_\eta(\mathbf{x}') \partial_{\mathbf{x}'} V(|\mathbf{x} - \mathbf{x}'|). \end{aligned} \quad (29)$$

Thus, this sum over  $\eta$  is introduced into Eq. (28) to obtain a force representation related to the lattice Boltzmann force that means also a sum over neighboring lattice sites:

$$\begin{aligned} \tilde{\mathbf{F}}(\zeta, t) &= \int d\mathbf{x} \rho(\mathbf{x}) \Delta_\zeta(\mathbf{x}) \\ &\times \sum_\eta \int d\mathbf{x}' \rho(\mathbf{x}') \Delta_\eta(\mathbf{x}') \partial_{\mathbf{x}'} V(|\mathbf{x} - \mathbf{x}'|). \end{aligned} \quad (30)$$

However, this is only an instantaneous force. A lattice Boltzmann (or lattice gas) method has a finite time step  $\Delta t$ , and the forcing term includes all the momentum absorbed during this finite time-step [42]. The total amount of momentum  $\mathbf{a}$  obtained is then:

$$\mathbf{a}(\zeta, T) = \int_{T\Delta t}^{(T+1)\Delta t} \tilde{\mathbf{F}}(\zeta, t) dt, \quad (31)$$

where  $T$  is the integer time of the simulation.

This is a fluctuating quantity, since it depends on the microscopic details of initial particle occupation. The next step is the application of the Boltzmann average, to look to all possible distributions that are compatible with the given macroscopic state. The definition of the probability of finding a particular configuration is then assumed to follow some local equilibrium assumption.

$$\tilde{\mathbf{a}} = \langle \mathbf{a}(\zeta, T) \rangle = \int d\rho(\mathbf{x}, t) P(\rho(\mathbf{x}, t)) \mathbf{a}(\zeta, T). \quad (32)$$

In an isothermal equilibrium system, the probability for a configuration  $\rho(\mathbf{x})$  would be given by:

$$P(\rho(\mathbf{x})) = \frac{1}{Z} e^{-\frac{H(\rho(\mathbf{x}))}{k_B T}}, \quad (33)$$

where  $H(\rho(\mathbf{x}))$  is the energy associated with the configuration  $\rho(\mathbf{x})$ ,  $k_B$  is the Boltzmann constant and  $T$  the temperature.  $Z$  is the partition function. In a general non-equilibrium situation, however, finding the probability of a density configuration is more challenging. Nonetheless, it is usual to make the assumption of local equilibrium for each lattice site, i.e. assuming that the particle configurations are in (or very close to) a local-equilibrium configuration with the constraint of the coarse-grained lattice densities at different lattice sites, which will be out of equilibrium.

Analytically deriving a force using Eq. (32) is a difficult computational task which we leave to a future publication. Here we want to point to a feature that appears when the size of the lattice is much larger than the interparticle interaction range and the mean-square displacement during a timestep  $\Delta t$  is likewise much smaller than that a lattice site, as is common in macroscopic and mesoscopic lattice Boltzmann applications: in this case the term  $\mathbf{a}$  only depends on a close neighborhood of lattice sites around the site we are considering.

We therefore propose, as an Ansatz, a general force for LB as expressed by Eq. (34) which preserves the locality of the forcing term predicted by (32). Like the standard

Shan-Chen approach this force contains the interaction potential function  $\psi = \psi(\rho)$  which can be adjusted to obtain the desired pressure tensor given by Eq. (10):

$$F_\alpha = \sum_i \sum_j A_{ij} \psi(\rho(\mathbf{x} + \mathbf{c}_i)) \psi(\rho(\mathbf{x} + \mathbf{c}_j)). \quad (34)$$

As in the original Shan-Chen approach the function  $\psi$  and the tensor  $A_{ij}$  are then adjusted, such that we obtain the desired expression of pressure tensor, Eq. (10). It should be noted that, in contrast to the approaches by [16, 18], the general force field represented by Eq. (34) is formulated considering the nearest-neighbor lattices only.

## B. Interaction potential moments

The pressure tensor, Eq. (13), is composed by the interaction potential function and its spatial derivatives. Thus, any attempt to evaluate it shall inevitably involve some numerical approximations for these derivatives. One of the simplest procedures would be using finite difference stencils to perform these approximations. A deeper and thorough explanation about these can be found in any classic finite difference method textbook [43]. By analyzing Eq. (21), one may realize that the numerical scheme of the Shan-Chen force can be interpreted as calculating the discrete first order moment of the term  $\psi(\mathbf{x} + \mathbf{c}_i)$ . In this section, a procedure to obtain the finite difference schemes written in the notation of these moments will be presented.

As only nearest-neighbor interactions are being considered, for the position  $\mathbf{x}$ , the operations must be done only with the values of the interaction potential  $\psi(\mathbf{x} + \mathbf{c}_i)$ . The Taylor series expansion of this term is given as follow:

$$\begin{aligned} \psi(\mathbf{x} + \mathbf{c}_i) &= \psi(\mathbf{x}) + c_{i\alpha} \partial_\alpha \psi(\mathbf{x}) + \frac{1}{2} c_{i\alpha} c_{i\beta} \partial_\alpha \partial_\beta \psi(\mathbf{x}) \\ &+ \frac{1}{6} c_{i\alpha} c_{i\beta} c_{i\gamma} \partial_\alpha \partial_\beta \partial_\gamma \psi(\mathbf{x}) + \dots \end{aligned} \quad (35)$$

In Eq. (35), one may observe that in each of the right-hand side terms, there is a polynomial in variables related to the lattice velocities. As for example, the first three terms involves, respectively, 1,  $c_{i\alpha}$  and  $c_{i\alpha} c_{i\beta}$ . Since it is a common practice to represent functions by discrete Hermite expansions in the LBM literature, it would be very convenient to rewrite the terms of Eq. (35) in the following form:

$$\begin{aligned} w_i \psi(\mathbf{x} + \mathbf{c}_i) &= w_i \left[ M^0 + \frac{c_{i\alpha}}{c_s^2} M_\alpha^1 + \frac{c_{i\alpha} c_{i\beta} - c_s^2 \delta_{\alpha\beta}}{2c_s^4} M_{\alpha\beta}^2 \right. \\ &\left. + \dots \right]. \end{aligned} \quad (36)$$

The moments of  $w_i \psi(\mathbf{x} + \mathbf{c}_i)$  are given by the following relations:

$$M^0 = \sum_i w_i \psi(\mathbf{x} + \mathbf{c}_i) \approx \psi(\mathbf{x}) + \frac{c_s^2}{2} \Delta \psi(\mathbf{x}), \quad (37a)$$

$$M_\alpha^1 = \sum_i w_i c_{i\alpha} \psi(\mathbf{x} + \mathbf{c}_i) \approx c_s^2 \partial_\alpha \psi(\mathbf{x}) + \frac{c_s^4}{2} \partial_\alpha \Delta \psi(\mathbf{x}), \quad (37b)$$

$$M_{\alpha\beta}^2 = \sum_i w_i (c_{i\alpha} c_{i\beta} - c_s^2 \delta_{\alpha\beta}) \psi(\mathbf{x} + \mathbf{c}_i) \approx c_s^4 \partial_\alpha \partial_\beta \psi(\mathbf{x}). \quad (37c)$$

It is worth mentioning that, when using the D2Q9 lattice, there are nine linearly independent discrete Hermite polynomials. In Eq. (36), only six of them were used, since they suffice for the purposes of the present work.

## C. Developing a force approach

As discussed in section (II B), the terms of the pressure tensor controls the multi-phase properties of the pseudopotential method. In particular, the following terms are useful:

$$p_{\alpha\beta}^{(1)} = (\partial_\gamma \psi)(\partial_\gamma \psi) \delta_{\alpha\beta}, \quad (38a)$$

$$p_{\alpha\beta}^{(2)} = \psi \partial_\alpha \partial_\beta \psi - (\psi \partial_\gamma \partial_\gamma \psi) \delta_{\alpha\beta}. \quad (38b)$$

The term  $p_{\alpha\beta}^{(1)}$  affects directly the value of the parameter  $\epsilon$  in Eq. (15), influencing the shape of the saturation curve. On the other hand the pressure  $p_{\alpha\beta}^{(2)}$  is related with surface tension, because the first term of the right hand side of Eq. (38b) is anisotropic. Note that this term also do not affect the  $\epsilon$  parameter, thus not changing the density relation for the planar interface. In such way, by introducing these terms, the deficiencies of Shan-Chen method can be corrected. These pressure terms can be converted in equivalent forces in the macroscopic governing equations using the relations:

$$F_\alpha^{(1)} = -\partial_\beta p_{\alpha\beta}^{(1)} = -2(\partial_\beta \psi)(\partial_\alpha \partial_\beta \psi), \quad (39a)$$

$$F_\alpha^{(2)} = -\partial_\beta p_{\alpha\beta}^{(2)} = -\partial_\beta [\psi \partial_\alpha \partial_\beta \psi - (\psi \partial_\gamma \partial_\gamma \psi) \delta_{\alpha\beta}]. \quad (39b)$$

Using the tensor identity, Eq. (12), it is possible to rewrite Eq. (39b) to the following form:

$$\begin{aligned} F_\alpha^{(2)} &= -\partial_\beta [(\partial_\gamma \psi)(\partial_\gamma \psi) \delta_{\alpha\beta} - (\partial_\alpha \psi)(\partial_\beta \psi)] \\ &= (\partial_\alpha \psi)(\partial_\beta \partial_\beta \psi) - (\partial_\beta \psi)(\partial_\alpha \partial_\beta \psi). \end{aligned} \quad (40)$$

Now that it was obtained explicit expressions for the interaction forces, it is necessary to replace the spatial derivatives for numerical approximations. This can be done with the moments defined by Eqs. (37a), (37b) and (37c). Truncating the series in its first term and replacing the derivatives, the following expressions are obtained:

$$F_\alpha^{(1)} = -2 \frac{M_\beta^1}{c_s^2} \frac{M_{\alpha\beta}^2}{c_s^4}, \quad (41a)$$

$$F_\alpha^{(2)} = \frac{M_\alpha^1 M_{\beta\beta}^2}{c_s^2 c_s^4} - \frac{M_\beta^1 M_{\alpha\beta}^2}{c_s^2 c_s^4}. \quad (41b)$$

Comparing Eq. (37a) and (37c) it can be concluded that another option is to use  $M_{\beta\beta}^2 = 2c_s^2(M^0 - \psi)$ . Eq. (41a) and (41b) are very useful and can be used to improve the Shan-Chen pseudopotential method to achieve thermodynamic consistency and adjustable surface tension. Based on this finding, the force term showed in Eq. (42) is proposed:

$$F_\alpha = F_\alpha^{SC} - \frac{3}{4}\epsilon c_s^2 G F_\alpha^{(1)} + (\sigma - 1) c_s^2 G F_\alpha^{(2)}. \quad (42)$$

This force represents the general force proposed in Sec. III A. The tensor  $A_{ij}$  is derived as follow. Expressing the fitting potential function as  $\psi(\mathbf{x}) = \psi(\mathbf{x} + \mathbf{c}_0)$  with  $\mathbf{c}_0 = 0$ , one can write:

$$\psi(\mathbf{x} + \mathbf{c}_0) = \sum_j \psi(\mathbf{x} + \mathbf{c}_j) \delta_{j0}. \quad (43)$$

The Shan-Chen force, Eq. (23), can be rewritten as:

$$F_\alpha^{SC} = \sum_i \sum_j \left[ -\frac{2G}{c_s^2} w_i \delta_{j0} \right] \psi(\mathbf{x} + \mathbf{c}_i) \psi(\mathbf{x} + \mathbf{c}_j). \quad (44)$$

Combining Eqs. (37b) and (37c) with Eq. (41a) results:

$$\begin{aligned} F_\alpha^{(1)} &= -2 \left[ \sum_i \frac{w_i}{c_s^2} c_{i\beta} \psi(\mathbf{x} + \mathbf{c}_i) \right] \\ &\quad \times \left[ \sum_j \frac{w_j}{c_s^4} (c_{j\alpha} c_{j\beta} - c_s^2 \delta_{\alpha\beta}) \psi(\mathbf{x} + \mathbf{c}_j) \right], \\ F_\alpha^{(1)} &= \sum_i \sum_j \left[ -2 \frac{w_i w_j}{c_s^2 c_s^4} c_{i\beta} (c_{j\alpha} c_{j\beta} - c_s^2 \delta_{\alpha\beta}) \right] \\ &\quad \times \psi(\mathbf{x} + \mathbf{c}_i) \psi(\mathbf{x} + \mathbf{c}_j). \end{aligned} \quad (45)$$

Now noting that the second term of the right side of Eq. (41b) is equal to  $F_\alpha^{(1)}/2$  and that the first term can be calculated with the help of Eqs. (37b) and (37c) as follows:

$$\begin{aligned} \frac{M_\alpha^1 M_{\beta\beta}^2}{c_s^2 c_s^4} &= \left[ \sum_i \frac{w_i}{c_s^2} c_{i\alpha} \psi(\mathbf{x} + \mathbf{c}_i) \right] \\ &\quad \times \left[ \sum_j \frac{w_j}{c_s^4} (c_{j\beta} c_{j\beta} - c_s^2 \delta_{\beta\beta}) \right], \\ &= \sum_i \sum_j \left[ \frac{w_i w_j}{c_s^2 c_s^4} c_{i\alpha} (c_{j\beta} c_{j\beta} - c_s^2 \delta_{\beta\beta}) \right] \\ &\quad \times \psi(\mathbf{x} + \mathbf{c}_i) \psi(\mathbf{x} + \mathbf{c}_j). \end{aligned} \quad (46)$$

The term  $F_\alpha^{(2)}$  is formulated as:

$$\begin{aligned} F_\alpha^{(2)} &= \sum_i \sum_j \frac{w_i w_j}{c_s^2 c_s^4} \left[ c_{i\alpha} (c_{j\beta} c_{j\beta} - c_s^2 \delta_{\beta\beta}) \right. \\ &\quad \left. - c_{i\beta} (c_{j\alpha} c_{j\beta} - c_s^2 \delta_{\alpha\beta}) \right] \psi(\mathbf{x} + \mathbf{c}_i) \psi(\mathbf{x} + \mathbf{c}_j), \end{aligned} \quad (47)$$

substituting the above relations into the Eq. (42), the  $A_{ij}$  tensor from Eq. (34) can be determined:

$$\begin{aligned} A_{ij} &= -\frac{2G}{c_s^2} w_i \delta_{j0} \\ &+ \left[ \frac{3}{2}\epsilon - (\sigma - 1) \right] c_s^2 G \frac{w_i w_j}{c_s^2 c_s^4} c_{i\beta} (c_{j\alpha} c_{j\beta} - c_s^2 \delta_{\alpha\beta}) \\ &+ (\sigma - 1) c_s^2 G \frac{w_i w_j}{c_s^2 c_s^4} c_{i\alpha} (c_{j\beta} c_{j\beta} - c_s^2 \delta_{\beta\beta}). \end{aligned} \quad (48)$$

When the above force is incorporated into the lattice Boltzmann equation using the Guo *et al.* force scheme, it results in the following pressure tensor in the momentum conservation equation:

$$p_{\alpha\beta} = p_{\alpha\beta}^{SC} - \frac{3}{4}\epsilon c_s^2 G p_{\alpha\beta}^{(1)} + (\sigma - 1) c_s^2 G p_{\alpha\beta}^{(2)}, \quad (49)$$

using Eqs. (25), (38a) and (38b) in the above relation it is obtained the final expression:

$$\begin{aligned} p_{\alpha\beta} &= \left( c_s^2 \rho + G \psi^2 - \frac{3}{4}\epsilon c_s^2 G (\partial_\gamma \psi) (\partial_\gamma \psi) \right. \\ &\quad \left. + \left( \frac{3}{2} - \sigma \right) c_s^2 G \psi \partial_\gamma \partial_\gamma \psi \right) \delta_{\alpha\beta} \\ &\quad + \sigma c_s^2 G \psi \partial_\alpha \partial_\beta \psi. \end{aligned} \quad (50)$$

The force was written in such a way that the parameter  $\epsilon$ , Eq. (18), of the consistency condition appears explicitly. This way, it is easy to adjust the coexistence curve and then control the surface tension through the coefficient  $\sigma$  of the anisotropic term of the pressure tensor Eq. (50).

## IV. NUMERICAL SIMULATIONS

### A. Static droplet and coexistence curve

The first aspect of the presented model that is tested is the ability of control the coexistence curve of the pseudopotential method by the choice of the parameter  $\epsilon$ . Numerical simulations were performed using Carnahan-Starling (C-S) equation of state:

$$P_{EOS} = k \left[ c \rho T \frac{1 + b\rho + (b\rho)^2 - (b\rho)^3}{(1 - b\rho)^3} - a\rho^2 \right], \quad (51)$$

the parameters were chosen to be  $a = 3.852462257$ ,  $b = 0.1304438842$  and  $c = 2.785855166$  which are the same values used in reference [11]. These authors introduced the scaling factor  $k$  in Eq. (51), which can also be used to increase the stability of the pseudopotential method [44]. This parameter is set as  $k = 0.01$ . Following [25], the computational domain is given by a mesh of  $200 \times 200$  nodes with periodic boundary condition. A liquid droplet is initialized in the center of the domain using the function:

$$\rho(x, y) = \frac{\rho_l + \rho_g}{2} - \frac{\rho_l - \rho_g}{2} \tanh \left[ \frac{2(R - R_0)}{W} \right], \quad (52)$$

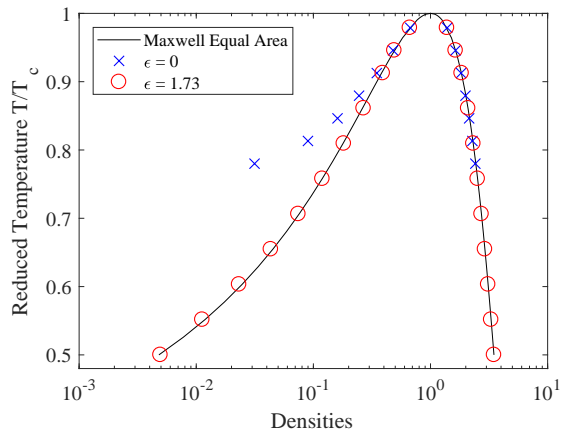


FIG. 1. Coexistence densities curves for planar interface. Comparison between results obtained with the lattice Boltzmann simulations for two values of the  $\epsilon$  parameter and the results obtained analytically with the Maxwell equal area rule.

where  $W = 5$  and  $R = \sqrt{(x - x_0)^2 + (y - y_0)^2}$ , with  $(x_0, y_0)$  being the central position of the computational domain. For a specific temperature, the values of  $\rho_g$  and  $\rho_l$  are initialized as the saturation densities obtained with Maxwell equal area rule. The velocity was set as zero everywhere. With the initialization of macroscopic fields, the equilibrium distribution function, Eq. (4), is determined in each lattice and the particle distribution function is set as equal to the equilibrium function. The lattice Boltzmann equation was solved using the BGK collision operator, Eq. (3a), with  $\tau = 0.8$ . Simulations were carried until the following convergence criteria has been obeyed:

$$\frac{\sum |\rho(t) - \rho(t - 100)|}{\sum |\rho(t)|} < 10^{-6}. \quad (53)$$

Setting  $G = -1$ ,  $\epsilon = 0$ ,  $\sigma = 1$  in Eq. (42), simulations were performed for different temperatures. One can notice that using these parameters is equivalent to use the original Shan-Chen force, Eq. (21). Then, the value of  $\epsilon$  is adjusted until the saturation curve of the pseudopotential method matches with the one given by the equal area rule. The value  $\epsilon = 1.73$  was found to provide this adjustment. Results can be seen in Fig. (1).

## B. Young-Laplace Test

In order to evaluate the influence of the parameter  $\sigma$  in the surface tension, further static droplet simulations were performed. The numerical procedure is similar to the ones used to produce the coexistence curve with the difference that all tests are conducted with a fixed temperature of  $T_r = 0.8$  and fixed  $\epsilon$  of value 1.73. Then the parameter  $\sigma$  is specified and when the droplet reaches an

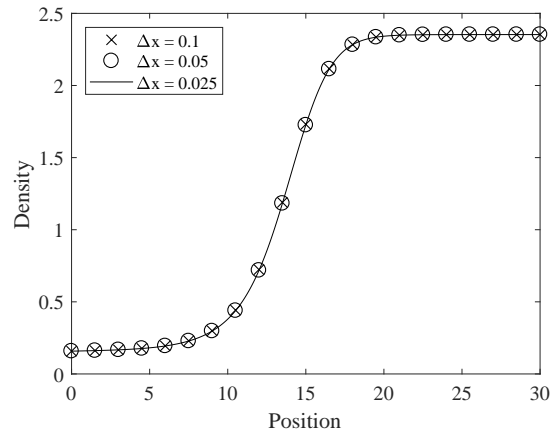


FIG. 2. Theoretical density profile for a planar interface case. It was adopted  $\epsilon = 1.73$  and a reduced temperature of  $T_r = 0.8$ . Boundary conditions were  $\rho_g = 0.1580$  and  $\rho_l = 2.3530$ .

equilibrium stage, the surface tension is measured using:

$$\Delta P = \gamma \left( \frac{1}{R_1} + \frac{1}{R_2} \right), \quad (54)$$

also known as the Young-Laplace relation. Fixing  $\sigma$ , simulations are performed for different radius and it is expected that the surface tension to remain constant. In the end, all this procedure is repeated for different values of  $\sigma$ . In Eq. (54),  $\gamma$  is the surface tension,  $\Delta P$  is the pressure difference across the interface. The parameters  $R_1$  and  $R_2$  are the radius of curvature of the interface. In the present case of a planar (2 dimension) droplet, there is only one radius of curvature equal to the radius of the droplet. In order to measure the radius, it was defined that the interface of the droplet was located in the region that the density is equal to  $\rho_m = (\rho_l + \rho_g)/2$ .

In order to obtain a comparison for the lattice Boltzmann simulation results, the surface tension of the planar interface case was computed using the procedure described in the end of Sec. II B. Eq. (14a) was solved numerically to obtain the density profile. One should note that this equation depends only on the values of  $A_1$  and  $A_2 + A_3$ , which are given by Eq. (50), being  $A_1 = -3\epsilon c_s^2/4$  and  $A_2 + A_3 = 3\epsilon c_s^2/2$ . In this way the density profile does not depend on the  $\sigma$  parameter, which influences only the surface tension value by the coefficient  $A_3$  in Eq. (20), given by  $A_3 = \sigma c_s^2$ . The boundary conditions used are the phase densities. For a reduced temperature  $T_r = 0.8$  and  $\epsilon = 1.73$ , Eq. (15) provide  $\rho_g \approx 0.1580$  and  $\rho_l \approx 2.3530$  as the vapor and liquid densities, respectively. A spatial domain of length  $L = 30$  was used and the differential equation was solved using three different mesh sizes  $\Delta x = 0.1$ ,  $\Delta x = 0.05$  and  $\Delta x = 0.025$ . The density profile is shown in Fig. (2). It can be observed convergence of results since the profiles are very close even with the mesh refinement.

After that the surface tension was computed using Eq. (20). It was obtained that the surface tension for

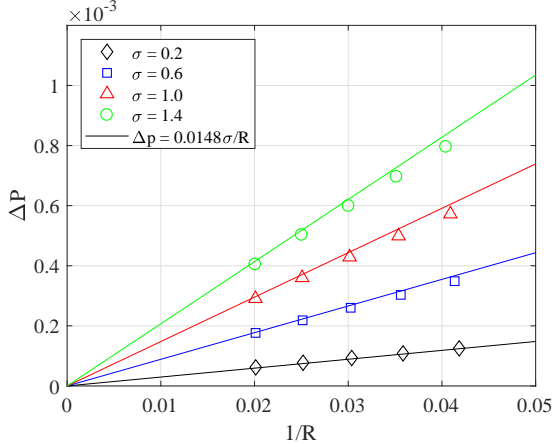


FIG. 3. Young-Laplace tests for static droplet with  $\sigma$  varying from 0.2 to 1.4 are performed for  $\epsilon = 1.73$  and reduced temperature  $T_r = 0.8$ . The solid lines represents the theoretical surface tension for a planar interface  $\gamma_{pi}(\sigma)$ .

a planar interface  $\gamma_{pi}$  is given by the expression  $\gamma_{pi} \approx 0.0148\sigma$ , for the specified conditions. A comparison between this results with the Young-Laplace test can be seen in Fig. (3). It is expected a small difference between the surface tension values obtained with the droplet and the planar interface tests because for the second case, the density profile is obtained considering that the pressure is constant along the normal direction to the interface. This is not true for the static droplet case. However, for large droplet radius, one may expect a better agreement in results, since the interface curvature tends to zero, which approximates the case to a planar interface problem. And this is exactly the behavior observed in Fig. (3). For a radius of 50 lattice sites, which corresponds to  $1/R = 0.02$ , the results of both cases were very close. It was also observed that the method succeeds in controlling the surface tension by adjusting the parameter  $\sigma$ .

The force term, Eq. (42), was devised in such a way that the surface tension could be adjusted without affecting the coexistence densities. In order to test this property, further tests were performed. The static droplet was simulated in a similar way as previous examples, but in this case, it was set  $T_r = 0.8$ ,  $\epsilon = 1.73$ ,  $R_0 = 50$  (initial radius of the droplet) and only  $\sigma$  was varied. For each test, the surface tension and the densities of the liquid and gas phases were measured. The results can be seen in Table (I). A comparison was carried out between the surface tension obtained by simulations ( $\gamma$ ) with the planar interface theoretical value ( $\gamma_{pi}$ ), for the same reduced temperature and  $\epsilon$  parameter. Also, the phase densities results were compared with the ones obtained by the Maxwell equal area rule, which are given by  $\rho_{gm} = 0.1665$  and  $\rho_{lm} = 2.3550$  for the vapor and liquid phase, respectively. On Table (I), it is observed that the surface tension can be widely varied without affecting

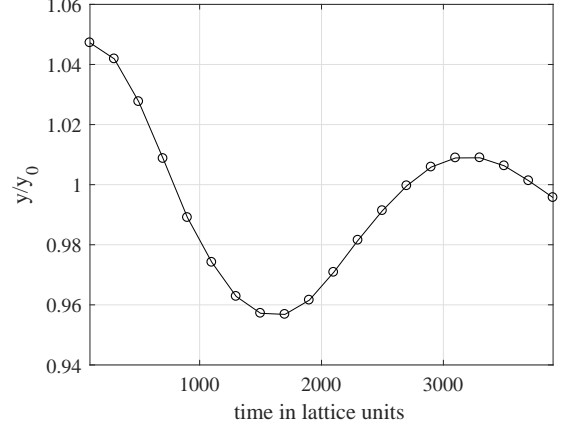


FIG. 4. Oscillation of an elliptic droplet for a fluid modelled by the C-S equation of state with reduced temperature  $Tr = 0.6$ .

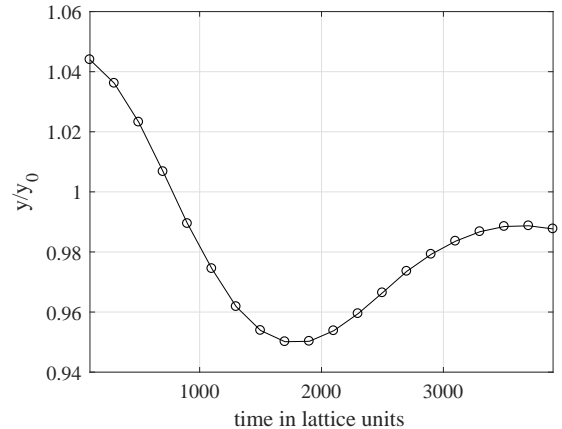


FIG. 5. Oscillation of an elliptic droplet for a fluid modelled by the C-S equation of state with reduced temperature  $Tr = 0.7$ .

significantly the phase densities.

### C. Droplet Oscillation

The next case is a dynamic test. It consists in a elliptic droplet oscillating in a vapor medium. Here, the C-S equation of state was used again. Two simulations were conducted, for the reduced temperatures  $T_r = 0.6$  and  $T_r = 0.7$ . The surface tension values and the phase densities for these reduced temperatures can be seen in Table (II). The Young-Laplace test was applied to obtain the values of the surface tension.

It is desired to initialize an elliptic profile of major radius  $R_{max} = 30$  and minor radius  $R_{min} = 27$  in a  $200 \times 200$  grid. As the pseudopotential method is a diffuse interface technique, a diffuse profile is initialized using Eq. (52). But now  $R_o$  is a function of space coordinates

TABLE I. Comparison between the variation of the surface tension with the variation of the liquid and vapor densities, obtained with the adjust of the parameter  $\sigma$  for a droplet of radius  $R = 50$  modelled by the C-S equation of state with a reduced temperature  $T_r = 0.8$ . It was also presented the theoretical surface tension value for a planar interface  $\gamma_{pi}$  and a comparison between the phase densities obtained by simulations with the vapor and liquid densities consistent with the Maxwell equal area rule, given by  $\rho_{gm} = 0.1665$  and  $\rho_{lm} = 2.3550$ .

$\sigma$	$\gamma$	$\gamma_{pi}$	$100 \cdot \gamma / \gamma_{pi}$	$\rho_g$	$100 \cdot \rho_g / \rho_{gm}$	$\rho_l$	$100 \cdot \rho_l / \rho_{lm}$
4	0.0603	0.0592	101.86	0.1595	95.80	2.3725	100.74
2	0.0290	0.0296	97.97	0.1658	99.58	2.3644	100.40
1	0.0145	0.0148	97.97	0.1688	101.40	2.3603	100.23
1/2	0.0074	0.0074	100.00	0.1704	102.34	2.3583	100.14
1/4	0.0039	0.0037	105.41	0.1711	102.76	2.3573	100.10
1/8	0.0020	0.00185	108.11	0.1715	103.00	2.3568	100.08

TABLE II. Saturation densities and surface tension obtained through static droplet test for the reduced temperatures  $T_r = 0.6$  and  $T_r = 0.7$  using the Carnahan-Starling (C-S) equation of state.

$T_r$	$\rho_g$	$\rho_l$	$\gamma$
0.6	0.0224	3.1192	0.0461
0.7	0.0700	2.7504	0.0267

$R_0 = R_0(x, y)$  and it is given by the following relations:

$$R_0(\theta) = \frac{R_{min}}{\sqrt{1 - (e \cos(\theta))^2}}, \quad (55a)$$

$$\theta(x, y) = \arctan\left(\frac{y - y_0}{x - x_0}\right), \quad (55b)$$

$$e = \sqrt{1 - \left(\frac{R_{min}}{R_{max}}\right)^2}, \quad (55c)$$

with  $(x_0, y_0)$  being the central position of the computational domain. The initial distribution function field is initialized equal to the equilibrium function  $f_i(t = 0, \mathbf{x}) = f_i^{eq}(t = 0, \mathbf{x})$ . It is clear that the initial state is not in equilibrium, so it is expected some error due to the chosen initialization procedure. To solve this case, it is used the lattice Boltzmann equation with the Gram-Schmidt based MRT collision operator, Eq. (3b). This option is based on the fact that this collision term is more stable at low viscosity, which is necessary in a dynamic test as viscosity dissipates perturbations rapidly. The force scheme used is given by Eqs. (5) and (6b). The relaxation matrix (more details in Appendix A) used is given by:

$$\Lambda = \text{diag}(1, 1, 1, 1, 1, 1, \tau^{-1}, \tau^{-1}), \quad (56)$$

here, it was used  $\tau = 0.65$  which results in a kinematic viscosity  $\nu = (\tau - 0.5)/3 = 0.05$ . The droplet oscillation period is given analytically, according to [45], by the relation:

$$T_a = 2\pi \left[ n(n^2 - 1) \frac{\gamma}{\rho_l R_m^3} \right]^{-\frac{1}{2}}, \quad (57)$$

where  $R_m = \sqrt{R_{max}R_{min}}$  and  $n = 2$  for an initial elliptic shape [34, 46]. The analytical result for  $T_r = 0.6$  is  $T_a \approx 3204$ . The simulation is conducted for 4000 time steps. The distance between the right extremity of the ellipse to its center is measured at each 100 time steps. The results are shown on Fig. (4). The numerical period of oscillation obtained is  $T_n = 3200$  which represents an absolute relative error of 0.1% of the analytical solution.

For the case with reduced temperature  $T_r = 0.7$  the droplet has a thicker interface width in comparison with the case for  $T_r = 0.6$ . In this way, it is expected a larger deviation in the solution. The analytical result using information from Table (II) is  $T_a \approx 3953$ . Again, the distance between the right extremity of the ellipse to its center is measured at each 100 time steps. The numerical period of oscillation is  $T_n = 3600$  which represents an absolute relative error of 9% of the analytical solution. Results are shown in Fig. (5).

## V. CONCLUSION

In the present work, an interaction force able to control the liquid-gas density ratio and the surface tension in the pseudopotential LBM was devised. First, the pressure tensor was written in a generic form and the role of each term was analyzed. Attention was paid to the property that different pressure tensors can result in the same divergence, reducing the number of terms necessary to describe the pressure tensor. After, the Shan and Chen model was studied by means of an equivalent pressure tensor including the third order spatial discretization errors caused by the Guo forcing scheme.

Later, it was presented finite difference approximations for the terms that constitute the pressure tensor. This approximations were written in the same notation as the moments of the distribution function. To devise the new interaction force, suitable terms of the generic pressure tensor were selected to complement the Shan and Chen model. Then it was derived an external force field able to replicate the effects of this pressure tensor terms in the conservation equations. This force field was converted into a numerical scheme using the finite difference ap-

proximations presented in Sec. III B. The result is a numerical force to be implemented into the LBM with the Guo forcing scheme.

Numerical simulations of a static droplet showed the ability of the method in control the liquid-gas density ratio and surface tension. Also, good results with dynamic tests were obtained. The proposed numerical scheme is versatile as the force was tested with BGK and MRT collision operator with no change in the procedure to calculate the external force. The new feature of this force is that it permits the control of these multi-phase properties considering only nearest-neighbor interactions, which provides computational efficiency in comparison with current interaction forces available in the literature.

### ACKNOWLEDGMENTS

The authors acknowledge the support received from CAPES (Coordination for the Improvement of Higher Education Personnel, Finance Code 001), from CNPq (National Council for Scientific and Technological Development, process 304972/2017-7) and FAPESP (São Paulo Foundation for Research Support, 2016/09509-1 and 2018/09041-5), for developing research that have contributed to this study.

### Appendix A: MRT Matrix

The MRT collision operator was presented in Eq. (3b). This operator depends on the matrix  $\mathbf{M}$  that converts the distribution functions into a set of linear independent moments. In this work it is used  $\mathbf{M}$  obtained by a Gram-Schmidt procedure [19] which is given by the following relation:

$$\mathbf{M} = \begin{pmatrix} 1 & 1 & 1 & 1 & 1 & 1 & 1 & 1 & 1 \\ -4 & -1 & -1 & -1 & -1 & 2 & 2 & 2 & 2 \\ 4 & -2 & -2 & -2 & -2 & 1 & 1 & 1 & 1 \\ 0 & 1 & 0 & -1 & 0 & 1 & -1 & -1 & 1 \\ 0 & -2 & 0 & 2 & 0 & 1 & -1 & -1 & 1 \\ 0 & 0 & 1 & 0 & -1 & 1 & 1 & -1 & -1 \\ 0 & 0 & -2 & 0 & 2 & 1 & 1 & -1 & -1 \\ 0 & 1 & -1 & 1 & -1 & 0 & 0 & 0 & 0 \\ 0 & 0 & 0 & 0 & 0 & 1 & -1 & 1 & -1 \end{pmatrix}, \quad (\text{A1})$$

while the relaxation matrix  $\mathbf{A}$  can be written as:

$$\mathbf{A} = \text{diag}(\tau_\rho^{-1}, \tau_e^{-1}, \tau_\zeta^{-1}, \tau_j^{-1}, \tau_q^{-1}, \tau_j^{-1}, \tau_q^{-1}, \tau_\nu^{-1}, \tau_\nu^{-1}). \quad (\text{A2})$$

The relaxation time  $\tau_\nu$  controls the fluid viscosity by the relation  $\mu = \rho c_s^2(\tau_\nu - 0.5)$ . A set of moments of the equilibrium distribution function  $\mathbf{m}^{eq}$  is obtained by multiplying the matrix  $\mathbf{M}$ , Eq. (A1), by the equilibrium distribution function vector,  $\mathbf{f}^{eq}$ , with components  $f_i = [\mathbf{f}^{eq}]_i$

given by Eq. (4):

$$\mathbf{m}^{eq} = \mathbf{M}\mathbf{f}^{eq} = \begin{pmatrix} \rho \\ -2\rho + 3\rho|\mathbf{u}|^2 \\ \rho - 3\rho|\mathbf{u}|^2 \\ \rho u_x \\ -\rho u_x \\ \rho u_y \\ -\rho u_y \\ \rho(u_x^2 - u_y^2) \\ \rho u_x u_y \end{pmatrix}, \quad (\text{A3})$$

and the force scheme in the moment space  $\bar{\mathbf{S}} = \mathbf{M}\mathbf{S}$  can be written as:

$$\bar{\mathbf{S}} = \mathbf{M}\mathbf{S} = \begin{pmatrix} 0 \\ 6(u_x F_x + u_y F_y) \\ -6(u_x F_x + u_y F_y) \\ F_x \\ -F_x \\ F_y \\ -F_y \\ 2(u_x F_x - u_y F_y) \\ u_x F_y + u_y F_x \end{pmatrix}. \quad (\text{A4})$$

### Appendix B: Tensor Identity

In Section II B, it was discussed how the divergence of different pressure tensors can lead to the same result. And an identity was provided by Eq. (12). In this appendix the given identity will be proven. The left-hand side of Eq. (12) is represented by Eq. (B1a) and the right-hand side by Eq. (B1b):

$$L_\alpha = \partial_\beta [\psi \partial_\alpha \partial_\beta \psi - (\psi \partial_\gamma \partial_\gamma \psi) \delta_{\alpha\beta}], \quad (\text{B1a})$$

$$R_\alpha = \partial_\beta [(\partial_\gamma \psi)(\partial_\gamma \psi) \delta_{\alpha\beta} - (\partial_\alpha \psi)(\partial_\beta \psi)], \quad (\text{B1b})$$

applying the sum rule for derivative and the fact that  $\partial_\beta(a)\delta_{\alpha\beta} = \partial_\alpha a$ , where  $a$  is a scalar:

$$L_\alpha = \partial_\beta (\psi \partial_\alpha \partial_\beta \psi) - \partial_\alpha (\psi \partial_\gamma \partial_\gamma \psi), \quad (\text{B2a})$$

$$R_\alpha = \partial_\alpha [(\partial_\gamma \psi)(\partial_\gamma \psi)] - \partial_\beta [(\partial_\alpha \psi)(\partial_\beta \psi)]. \quad (\text{B2b})$$

Now, applying the product rule for derivative, Eqs. (B2a) and (B2b) can be rewritten in the following way:

$$L_\alpha = \begin{aligned} & (\partial_\beta \psi)(\partial_\alpha \partial_\beta \psi) + \psi \partial_\alpha \partial_\beta \partial_\beta \psi \\ & - (\partial_\alpha \psi)(\partial_\gamma \partial_\gamma \psi) - \psi \partial_\alpha \partial_\gamma \partial_\gamma \psi, \end{aligned} \quad (\text{B3a})$$

$$R_\alpha = \begin{aligned} & 2(\partial_\gamma \psi)(\partial_\alpha \partial_\gamma \psi) - (\partial_\alpha \psi)(\partial_\beta \partial_\beta \psi) \\ & - (\partial_\beta \psi)(\partial_\alpha \partial_\beta \psi), \end{aligned} \quad (\text{B3b})$$

the dummy index  $\gamma$  can be replaced without affecting the results, so choosing  $\beta$  in its place:

$$L_\alpha = (\partial_\beta \psi)(\partial_\alpha \partial_\beta \psi) - (\partial_\alpha \psi)(\partial_\beta \partial_\beta \psi), \quad (\text{B4a})$$

$$R_\alpha = (\partial_\beta \psi)(\partial_\alpha \partial_\beta \psi) - (\partial_\alpha \psi)(\partial_\beta \partial_\beta \psi). \quad (\text{B4b})$$

Now, the equality is proven.

- 
- [1] S. Chen and G. D. Doolen, Annual review of fluid mechanics **30**, 329 (1998).
- [2] X. Shan and X. He, Physical Review Letters **80**, 65 (1998).
- [3] A. K. Gunstensen, D. H. Rothman, S. Zaleski, and G. Zanetti, Physical Review A **43**, 4320 (1991).
- [4] M. R. Swift, E. Orlandini, W. R. Osborn, and J. M. Yeomans, Physical Review E **54**, 5041 (1996).
- [5] X. Shan and H. Chen, Physical Review E **47**, 1815 (1993).
- [6] L.-S. Luo, Physical review letters **81**, 1618 (1998).
- [7] X. Shan and H. Chen, Physical Review E **49**, 2941 (1994).
- [8] D. M. Anderson, G. B. McFadden, and A. A. Wheeler, Annual review of fluid mechanics **30**, 139 (1998).
- [9] Q. Li, K. H. Luo, Q. Kang, Y. He, Q. Chen, and Q. Liu, Progress in Energy and Combustion Science **52**, 62 (2016).
- [10] R. Zhang and H. Chen, Physical Review E **67**, 066711 (2003).
- [11] A. Kupershtokh, D. Medvedev, and D. Karpov, Computers & Mathematics with Applications **58**, 965 (2009).
- [12] S. Gong and P. Cheng, Computers & Fluids **53**, 93 (2012).
- [13] S. Gong and P. Cheng, International Communications in Heat and Mass Transfer **87**, 61 (2017).
- [14] X. Ma and P. Cheng, International Journal of Heat and Mass Transfer **131**, 1095 (2019).
- [15] X. Shan, Physical Review E **73**, 047701 (2006).
- [16] M. Sbragaglia, R. Benzi, L. Biferale, S. Succi, K. Sugiyama, and F. Toschi, Physical Review E **75**, 026702 (2007).
- [17] Q. Li and K. H. Luo, Physical Review E **88**, 053307 (2013).
- [18] S. F. Kharmani, H. Niazmand, and M. Passandideh-Fard, Journal of Statistical Physics **175**, 47 (2019).
- [19] T. Krüger, H. Kusumaatmaja, A. Kuzmin, O. Shardt, G. Silva, and E. M. Vigen, Springer International Publishing **10**, 978 (2017).
- [20] M. R. Parsa and A. J. Wagner, Physical Review E **96**, 013314 (2017).
- [21] Z. Guo, C. Zheng, and B. Shi, Physical Review E **65**, 046308 (2002).
- [22] A. Kupershtokh, in *Proc. 5th International EHD Workshop, University of Poitiers, Poitiers, France* (2004) pp. 241–246.
- [23] A. J. Wagner, Physical Review E **74**, 056703 (2006).
- [24] Q. Li, K. H. Luo, and X. J. Li, Physical Review E **86**, 016709 (2012).
- [25] H. Huang, M. Krafczyk, and X. Lu, Physical Review E **84**, 046710 (2011).
- [26] D. Lycett-Brown and K. H. Luo, Physical Review E **91**, 023305 (2015).
- [27] R. Huang and H. Wu, Journal of Computational Physics **327**, 121 (2016).
- [28] Q. Zhai, L. Zheng, and S. Zheng, Physical Review E **95**, 023313 (2017).
- [29] Q. Li, Q. Kang, M. M. Francois, Y. He, and K. Luo, International Journal of Heat and Mass Transfer **85**, 787 (2015).
- [30] Q. Li, Y. Yu, P. Zhou, and H. Yan, Applied Thermal Engineering **132**, 490 (2018).
- [31] A. Hu and D. Liu, Applied Thermal Engineering **159**, 113788 (2019).
- [32] P. L. Bhatnagar, E. P. Gross, and M. Krook, Physical review **94**, 511 (1954).
- [33] G. Kaehler and A. J. Wagner, Communications in Computational Physics **13**, 614 (2013).
- [34] Q. Li, K. H. Luo, and X. J. Li, Physical Review E **87**, 053301 (2013).
- [35] Y.-T. Mu, L. Chen, Y.-L. He, Q.-J. Kang, and W.-Q. Tao, International Journal of Heat and Mass Transfer **106**, 708 (2017).
- [36] A. Wagner, *Theory and applications of the lattice Boltzmann method*, Ph.D. thesis, University of Oxford (1997).
- [37] D. J. Holdych, D. R. Noble, J. G. Georgiadis, and R. O. Buckius, Journal of Computational Physics **193**, 595 (2004).
- [38] P. Yuan and L. Schaefer, Physics of Fluids **18**, 042101 (2006).
- [39] X. Shan, Physical Review E **77**, 066702 (2008).
- [40] J. S. Rowlinson and B. Widom, *Molecular theory of capillarity* (Courier Corporation, 2013).
- [41] M. R. Parsa and A. J. Wagner, arXiv preprint arXiv:1905.07611 (2019).
- [42] Q. Li and A. J. Wagner, Physical Review E **76**, 036701 (2007).
- [43] R. J. LeVeque, *Finite difference methods for ordinary and partial differential equations: steady-state and time-dependent problems*, Vol. 98 (Siam, 2007).
- [44] A. Hu, L. Li, S. Chen, Q. Liao, and J. Zeng, International Journal of Heat and Mass Transfer **67**, 159 (2013).
- [45] H. Lamb, Dover, New York **4**, 18 (1932).
- [46] S. Mukherjee and J. Abraham, Computers & fluids **36**, 1149 (2007).